Superchiral Plasmonic Phase Sensitivity for Fingerprinting of Protein Interface Structure

Ryan Tullius,[†] Geoffrey W. Platt,[‡] Larousse Khosravi Khorashad,[§] Nikolaj Gadegaard,[‖] Adrian J. Lapthorn,[†] Vincent M. Rotello,[¦] Graeme Cooke, [†] Laurence D. Barron, [†] Alexander O. Govorov, [§] Affar S. Karimullah*,[†,‖], Malcolm Kadodwala*,[†].

[†] School of Chemistry, Joseph Black Building, University of Glasgow, Glasgow, G12 8QQ, UK.

[‡] Avacta Life Sciences, Ash Way, Thorp Arch Estate, Wetherby, LS23 7FA, UK.

[§] Department of Physics and Astronomy, Ohio University, Athens, Ohio 45701, USA

[‖] School of Engineering, Rankine Building, University of Glasgow, Glasgow, G12 8LT, UK.

[¦] Department of Chemistry, 710 Nt. Pleasant Street, University of Massachusetts Amherst, MA 01003, USA.

Abstract

The structure adopted by biomaterials, such as proteins, at interfaces is a crucial parameter in a range of important biological problems. It is a critical property in defining the functionality of cell / bacterial membranes, biofilms (*i.e.* in antibiotic resistant infections) and the exploitation of immobilised enzymes in biocatalysis. The intrinsically small quantities of materials at interfaces precludes the application of conventional spectroscopic phenomena routinely used for (bio)structural analysis due to a lack of sensitivity. We show that the

interaction of proteins with superchiral fields induces asymmetric changes in retardation phase effects of excited bright and dark modes of a chiral plasmonic nanostructure. Phase retardations are obtained by a simple procedure, which involves fitting the line shape of resonances in the reflectance spectra. These interference effects provide fingerprints, which are an incisive probe of the structure of interfacial biomolecules. Using these fingerprints, layers composed of structurally related proteins with differing geometries can be discriminated. Thus, we demonstrate a powerful tool for the bioanalytical toolbox.

Keywords: plasmonic, metamaterials, plasmonic induced transparency, biosensing, chiral

Biointerfaces play a key role in biology and biotechnology, providing the contact point between a biological system and the environment. The structure of biointerfaces, such as the orientation and higher order structure (*e.g.*tertiary) of constituent proteins and other macromolecular assemblies, is an important parameter that governs functionality. However, since interfacial regions intrinsically contain small amounts of material, conventional chirally sensitive spectroscopic tools, routinely applied to characterise biomaterials, cannot be used due to lack of sensitivity. Consequently, routine laboratory based characterisation of biointerfaces is generally provided by atomic force microscopy (AFM) which uses topographical and mechanical properties to establish the macromolecular shape of the molecules based on correlation averaged image reconstruction.[1,2] However, rapid detection of subtle structural and orientation differences between similar molecules with AFM can be challenging. Here we report a plasmonic phenomenon which is based on the sensitivity of phase retardation effects in plasmonic transparency on the spatial arrangement of protein molecules within the nearfield. Absorbed layers of biomolecules cause an asymmetry in

changes in phase retardation between left (LH) and right (RH) handed structures due to the differential interaction of chiral near fields with a chiral dielectric environment. Using this phenomenon, we have discriminated between layers formed from structurally related proteins that are spectroscopically indistinguishable in solution. A central concept of our work is superchiral electromagnetic fields, which locally display greater chiral asymmetry than circularly polarised plane light waves.[3,4] It has been already been demonstrated that optical excitation of chiral plasmonic nanostructures can generate nearfields which exhibit superchirality.[5–7] The hypothesis we propose for the current phenomena is that the asymmetry in phase retardation arises through the differential interaction of superchiral nearfields with a chiral dielectric. This behavior is analogous to the asymmetry in phase shifts that occur for LH and RH circularly polarised light (CPL) during propagation through chiral media.

Previously, chiral fields generated by plasmonic nanostructures have been applied to achieve chiral discrimination of small molecules and the detection of protein secondary structure through the measurement of asymmetries in the shifts of plasmonic resonances.[5,8–10] However, in the present study we show that superchiral retardation phase shifts are a more incisive probe of biological structure, being able to discriminate between layers consisting of structurally related proteins.

Retardation is the effect of the phase difference between fields propagating from spatially separated regions of a nanostructure, giving rise to phase changes in excited plasmon modes, and is important for analysing larger structures.[11–13] In the case of a chiral structure, the fields have chiral asymmetries which will differentially interact with a chiral dielectric giving rise to an asymmetry in retardation effects. In the current study we are able to determine retardation phase shifts from reflectance spectra from metamaterials which display plasmonic induced transparency.[14,15] This effect is an analogue of the quantum interference phenomenon

of electromagnetically induced transparency (EIT), referred to as plasmon induced transparency. EIT renders an opaque medium transparent in a narrow spectral region due to the destructive interference of two excitation pathways mediated by a laser-coupling field. In plasmonic induced transparency a dip is observed in the reflectance / transmission resonance.[16–18] The two states that are coupled in the metamaterials are typically optically bright dipolar and optically dark quadrupolar modes. The significant differences between EIT in atomic systems and plasmonic induced transparency are: coupling is achieved *via* near fields; and retardation effects become significant because the dimensions of nanostructures are comparable to the wavelength of light. Subtle variations in the nearfield, derived from the properties of the environment, lead to significant perturbations in the phase retardation effects that are measurable in coupled oscillator systems that display EIT behaviour. Put simply, the reported phenomenon can be considered a form of *superchiral plasmonic interferometry*. This application of superchiral fields provides information inaccessible to routine biophysical spectroscopic tools.

Results and Discussion

In this study we have used chiral plasmonic solid-inverse hybrid gold metafilms that have both bright (dipole) and dark (quadrupole) modes, and have previously been demonstrated to exhibit plasmonic induced transparency.[19,20] The origin and properties of the dipole and quadrupole modes of this nanostructure have been discussed previously.[19] As a planar metafilm, instead of an induced transmission peak, an enhanced reflectivity peak within a broader transmission/absorption profile is observed. [21,22] The metafilms are formed by depositing gold on nano-patterned polycarbonate templates, hence called templated plasmonic substrates (TPS),[23] that consist of "Shuriken" shaped indentations, with six fold rotational symmetry, of either LH or RH, arranged in a square lattice (further details in supplementary information 1.1). These nanostructures have previously been used to sense

chiral molecules and have shown opposite asymmetries for enantiomers (supplementary information 1.1).[10,19]

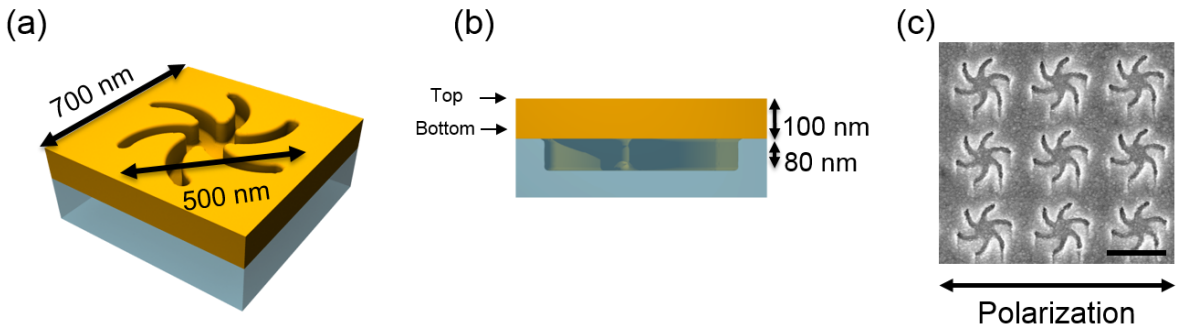

Figure 1: (a) Perspective image showing dimensions of a single shuriken nanostructure and (b) showing the depth profile and the positions of surfaces labelled top and bottom. (c) Electron microscopy images of a RH TPS of the nanostructure and polarization direction of the incident light (scale bar represents 500 nm).

In order to extract the retardation phase shifts from the reflectance spectra we introduce a simple classical model to describe plasmonic induced transparency. It is based on two coupled oscillators, and replicates reflectance spectra. Variations of this approach have been used in a number of studies.[16,24] The starting point is a model system that is described by a set of two coupled harmonic oscillators,

$$\omega_r{}^{-2}\,\ddot{p}(t) + \gamma_r\omega_r{}^{-1}\,\dot{p}(t) + p(t) = gf(t) - \tilde{\kappa}\,q(t) \qquad (1)$$

$$\omega_d{}^{-2}\,\ddot{q}(t) + \gamma_d\omega_d{}^{-1}\,\dot{q}(t) + q(t) = -\tilde{\kappa}\,p(t) \qquad (2)$$

Here the radiative (bright) resonator is described by the excitation *p(t)* with a resonance frequency ω_r and damping factor γ_r. Similarly, the dark mode excitation is described by *q(t)* with a resonance frequency ω_d and damping factor γ_d. The two resonators are coupled *via* a complex coupling constant κ. The bright mode is driven by an external force *f(t)* and *g* is a constant indicating the coupling strength between the oscillator and the external force. In contrast to previous applications of the coupled oscillator model to plasmonic transparency

we include terms $e^{i\theta}$ and $e^{i\phi}$ which account for retardation phase shifts, θ and ϕ, in the bright and dark mode excitations respectively. Both resonators are linearly coupled *via* a complex coupling coefficient $\tilde{\kappa} = \kappa e^{-i(\theta-\phi)}$. The solutions of (1) and (2) take the form,

$$p(t) = e^{-i\theta}P(\omega)e^{-i(\omega t)} \quad (3)$$

$$q(t) = e^{-i\phi}Q(\omega)e^{-i(\omega t)} \quad (4)$$

Using these equations and assuming an effective medium approximation, an expression for the reflectivity can be derived and used for fitting the experimental data. A full description of the fitting procedure and a complete list of the parameters required to fit the spectra are given in supplementary information 1.3 and 1.4.

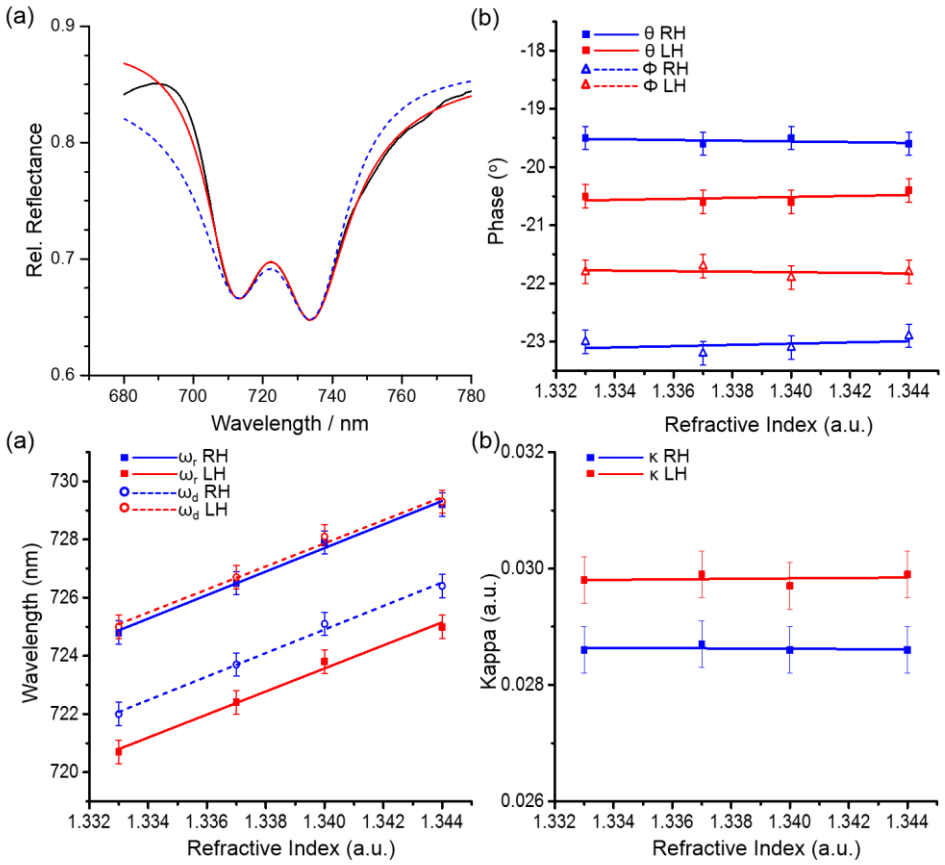

Figure 2: (a) Fitting results of reflectance with water (experimental, black) without phase differences being considered (blue dotted) and with introduction of phase (red) in the fitting equation. (b-d) show the

fitting results for θ, Φ , w_r,w_d and κ, from the salt solutions showing linear behaviour over differing RIs and no asymmetry between RH and LH TPSs.

For reference purposes we have collected, and subsequently fitted, reflectance spectra from LH and RH substrates in the presence of non-chiral solutions of increasing refractive index (RI) (**Figure 2** and supplementary information 1.4). It is important to note that reflectance spectra cannot be well fitted using a coupled oscillator model which does not take account of retardation phase shifts, **Figure 2(a)**. This is consistent with the relatively large nanostructures used in this study; previous work where plasmonic transparency could be modelled without the introduction of phase shifts used smaller nanostructures, for which retardation effects would be less significant.[16] The values of ω_r, ω_d, κ, θ and ϕ derived from the fits are plotted as a function of the RI of the solutions in **Figure 2(b-d)**. As expected LH and RH substrates exhibit qualitatively similar behaviour. The wavelengths of both ω_r and ω_d linearly increase with the RI of the solutions; within the precision of our measurements, both exhibit the same RI sensitivity, ~400 nm / RIU. Within the precision of the fitting routine κ, θ and ϕ shows no dependency on the RI of the salt solutions. The absence of any dependency of the retardation phase shifts θ and ϕ on the RI of the achiral salt solutions is readily reconciled within the framework of our hypothesis. Fields of both chiral asymmetry will interact equally with achiral (non-chiral) dielectrics. Consequently, only size effects contribute the observed retardation phase shifts.

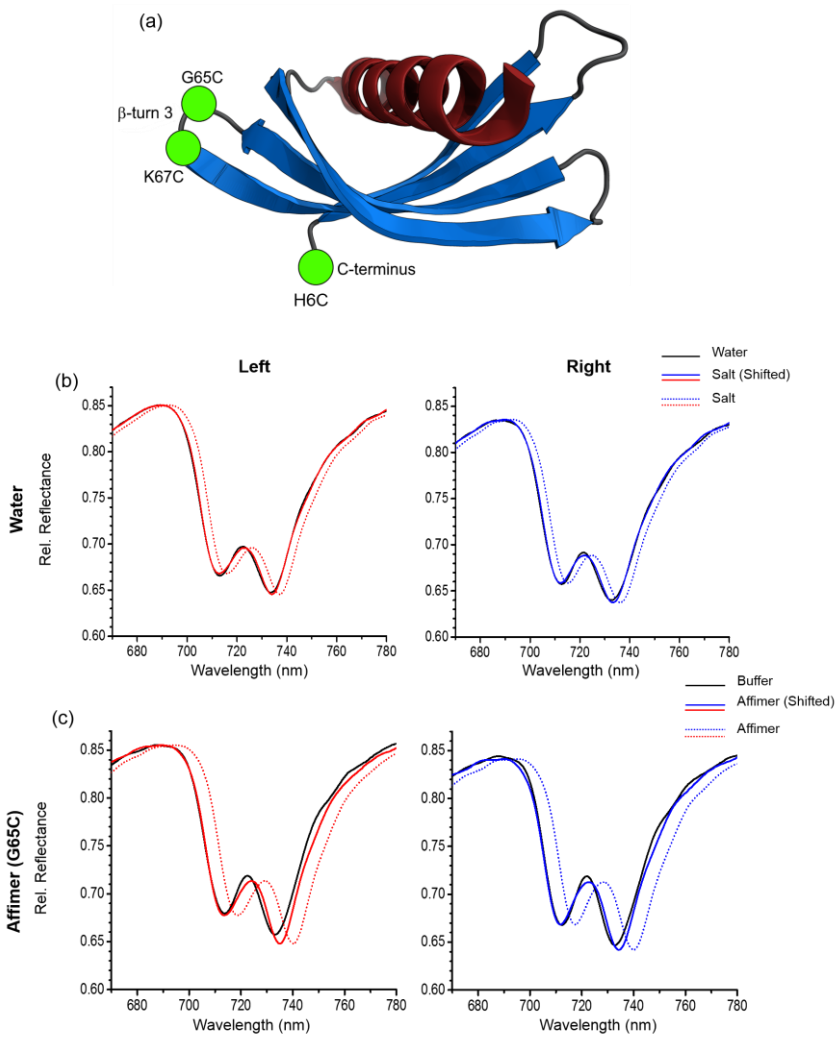

Figure 3: (a) Model of the Affimer protein scaffold (PDB accession code 4N6U)[25] labelled with the positions in β-turn 3 and the C-terminus where cysteine was added in order to bind the protein to the gold surface. Graphs for (b) reflectance with water (solid black) and salt solution (dotted coloured) with both LH (red) and RH (blue) TPS's. To aid comparison shifted salt solution spectra (solid colour line) are shown. (c) Reflectance spectra from substrates with absorbed Affimer (dotted coloured) and water (solid black) for LH (red) and RH (Blue) are displayed. Again, to aid comparison shifted Affimer spectra are also shown (solid coloured)

To demonstrate the structural incisiveness of phase sensitivity we have chosen a challenging exemplar system that will create layers of structurally similar protein (*i.e.* no significant differences in secondary and tertiary structure), which have been immobilised on to surface with different orientations. Crucially, discrimination between the protein layers cannot be achieved using measurements of the asymmetries in resonance wavelength shift ($\Delta\lambda_{L/R}$) on left and right handed substrates as used in previous studies. Such asymmetry parameters are sensitive to the secondary and tertiary structure of surface immobilized proteins.[5,10,26]

Thus we have used a class of recombinant non-antibody binding proteins, called Affimers that all share a common small tightly bundled protein scaffold which displays high thermal stability and undergo minimal structural deformation when immobilised on to surfaces (including Au). Attached to this protein scaffold by both ends are two identical variable loop regions which bind to a specific target. The amino acid sequences of the binding loops can be altered in a controlled manner to bind a particular target. A more detailed description of the protein structure can be found in supplementary information 1.5. We have used three variants of an Affimer protein (G65C, K67C and H6C) each engineered to have a single cysteine residue at a different position within the structure, as shown in **Figure 3(a)** and detailed in supplementary information 1.5. Both G65C and K67C were designed to bind the protein glutathione S-transferase (GST), while H6C binds the protein immunoglobulin G (IgG). Since the 79 amino acid sequence of the G65C and K67C mutants only differ by the position of a single cysteine residue they will have the most similar structures. The sequence of H6C has 19 amino acids different to G65C and K67C. Although the three Affimers have different amino acid sequences, this does not significantly affect higher order tertiary structure. This is verified with fluorescence data which indicates that the introduction of a cysteine residue into the protein and different binding loop sequences of H6C to G65C and K67C, has no large effect on the tertiary structure (supplementary information 1.5) and is consistent with literature.[25] The surface stability of the Affimer protein fold (tertiary structure) is well documented,[27,28] and is exploited in biosensing applications.[29–31] These three Affimer proteins can be immobilised onto the Au surface, through the thiol group of the cysteine residue. Single adsorbed layers of the Affimer mutants were deposited on to the metafilms (see methods) and spectra collected from this surface immersed in buffer. This immobilisation methodology has been used previously to create Affimer based biosensors for cancer relevant proteins.[29] The high binding affinity of the Affimers to their targets (see

supplementary information 1.5) observed in this previous study was indicative of a lack of significant perturbation in the secondary and tertiary protein structure, since any significant perturbation of Affimer structure, due to non-specific interactions with the surface, leads to a loss of affinity for the target. In addition to this loss of affinity, changes caused to the Affimer structures, as a result of surface binding to gold, would also potentially reduce or eliminate the specificity of the Affimer to its target protein.

The similarity in the structures of the three layers formed by the Affimers is furthers supported by an asymmetry parameter used in previous work,[5,10] the ΔΔλ asymmetry. The ΔΔλ is measured using the wavelength shifts of the peaks of the optical rotation dispersion (ORD) (see supplementary information 1.1 and 1.6). **Figure 5 (b)** shows the ΔΔλ values for the Affimers which are small and within experimental error of each other demonstrating the structural parallelism between the three Affimers.

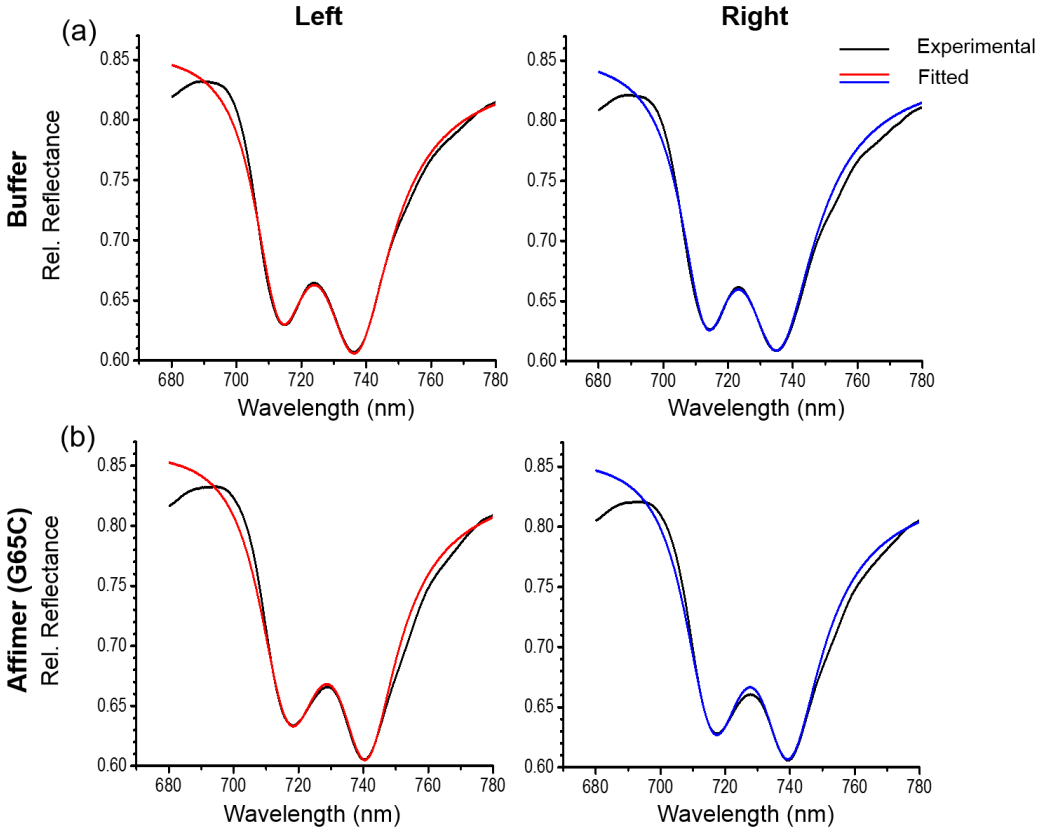

Figure 4: Fitting results for (a) buffer and (b) Affimer G65C, with black lines showing experimental data and the coloured lines showing fitted data for LH (red) and RH (blue) TPSs.

Experimental reflectance spectra for a salt solution and an Affimer (G65C) with similar RI were compared. While the salt solution shows no significant change in the reflectance shape, **Figure 3(b)**, it is clear that the presence of the Affimer layer has a significant effect on the shape of the reflectance peak, **Figure 3(c)**. The reflectance of buffer solutions and the subsequently added Affimer proteins were fitted using the plasmon induced transparency model. **Figure 4** shows the fitting results for Affimer G65C. Similar reflectance measurements and fitting were performed for Affimers K67C and H6C and the complete list of values for the fitting parameters are given in the supplementary information 1.6. Differences in the ω_r, ω_d, κ, θ and ϕ values between Affimer and buffer for LH and RH substrates have been calculated; from these asymmetry parameters are also derived, $\Delta\Delta x = {}^{R}\Delta x - {}^{L}\Delta x$ where $x = \omega_r$, ω_d, κ, θ and ϕ. The three Affirmer's have non-zero values for all the asymmetry parameters, indicating that the presence of the Affimer proteins differentially affects the reflectance properties of LH and RH substrates. Within experimental error, the set of values for $\Delta\Delta\omega_r$, $\Delta\Delta\omega_d$, and $\Delta\Delta\kappa$ are the same for all three Affimer proteins (supplementary information 1.6). However, it is noteworthy that the $\Delta\Delta\omega_r$ and $\Delta\Delta\omega_d$ have opposite signs and the latter has a larger magnitude (~ 1.5 times) than the former. In contrast to the other three parameters $\Delta\Delta\theta$ and $\Delta\Delta\phi$ values, **Figure 5 (a)**, do differ significantly for the three cases, providing a distinct fingerprint for the Affimer layer structure. This reflects the fact that the overall shapes of the reflectance spectra are far more sensitive to relatively small changes in retardation phases (θ and ϕ) than they are to equivalently small changes in ω_r and ω_d (see supplementary information 1.6). Furthermore, the inability of $\Delta\Delta\lambda$ to detect the small changes between the layers demonstrates the greater incisiveness of asymmetries in phase to the structure of biointerfaces.

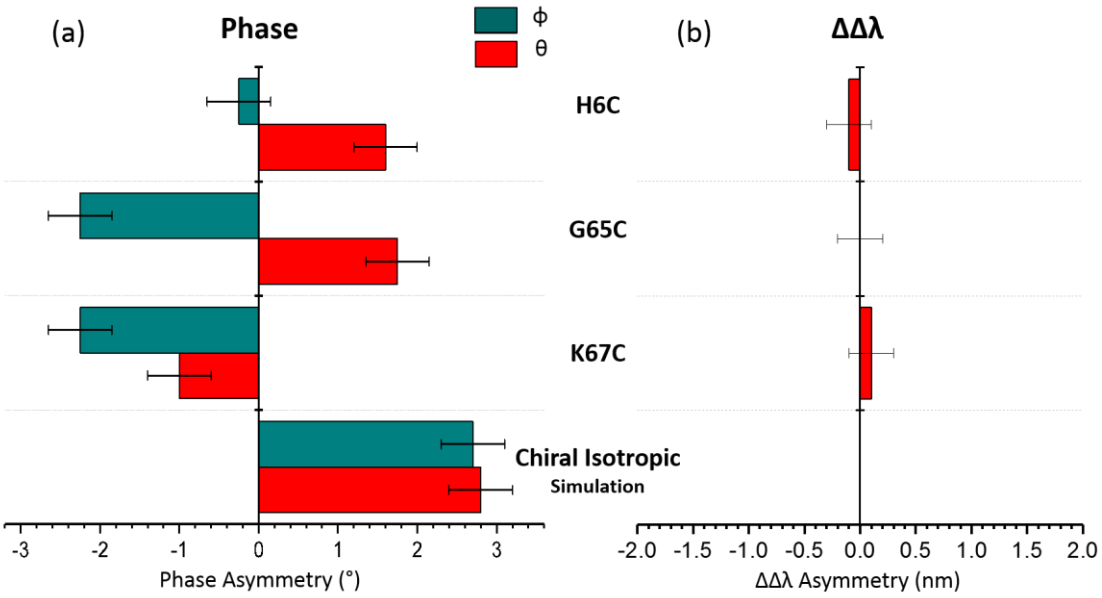

Figure 5: (a) Asymmetry in phase parameters (θ and Φ) for the Affimer proteins, and the simulated isotropic chiral layer. (b) ΔΔλ values taken by position of a peak from the ORD spectra for all three Affimers.

In order to validate the general concept that a chiral dielectric can cause an asymmetry in phase retardation which will be observed in reflectance spectra, numerical EM simulations were performed. The model simulated was a 20 nm thick isotropic chiral dielectric layer covering the shurikens. The chiral dielectric layer was modelled based on the constitutive equations for an isotropic chiral dielectric medium given by:[32,33]

$$\boldsymbol{D} = \varepsilon_o \varepsilon_r \boldsymbol{E} + i\xi \boldsymbol{B} \qquad (5)$$

$$\boldsymbol{H} = \boldsymbol{B}/\mu + i\xi \boldsymbol{E} \qquad (6)$$

Here, ε_o is the permittivity of free space, ε_r is the relative permittivity, μ is the permeability, $\boldsymbol{E}$ is the complex electric field, $\boldsymbol{B}$ is the complex magnetic flux density, $\boldsymbol{H}$ is the magnetic field, $\boldsymbol{D}$ is the electric displacement field and ξ is a local parameter descripting the chiral property of a molecular layer (more details in supplementary information 1.2). ξ is only non-

zero for a chiral dielectric. Following the procedure described by Govorov *et al.,*[34,35] it can be shown that for a protein layer $\xi \approx 5x10^{-4}$ (for a wavelength of 700 nm). The shuriken nanostructure is excited by linearly polarized light and an optical chirality parameter C (supplementary information 1.2), first described by Tang and Cohen,[4,36] has been used to parameterise the level of chiral asymmetry of the near fields, the spatial variation of optical chirality being shown in **Figure 6 (b)** . The shuriken nanostructures, excited with linearly polarized light, generate superchiral fields of both handedness, albeit with one in excess. The simulations successfully demonstrate changes to the reflectivity, **Figure 6 (a),** and were fitted with the coupled oscillator model to extract the phase parameters, **Figure 5 (a)** (a full list of parameter can be found in supplementary information 1.7). An asymmetry in phase parameters ϕ and θ is observed on going from LH and RH structures which is comparable in size to that observed in the experimental data.

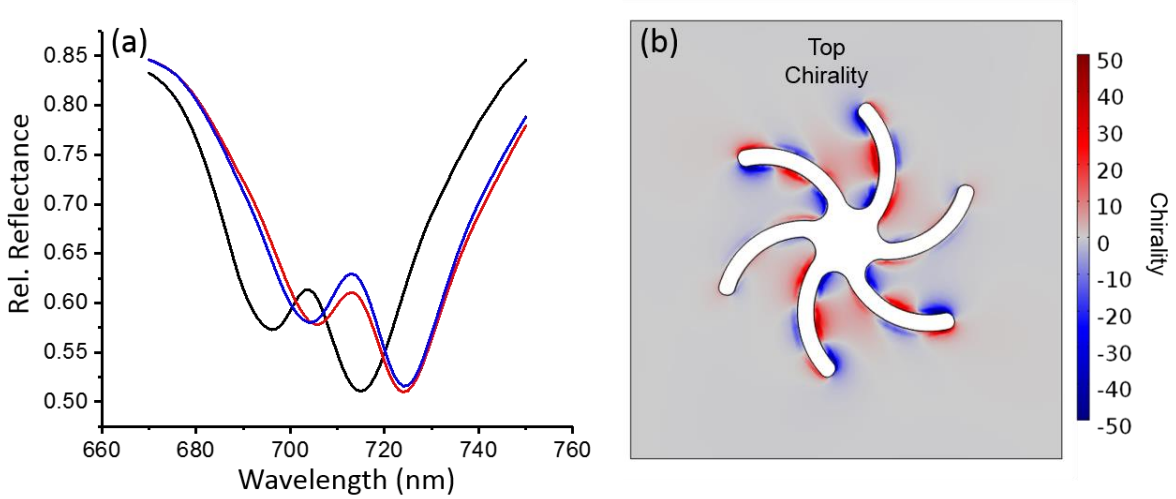

Figure 6: (a) Reflectance plot from simulations with chiral dielectric covered shuriken nanostructures, LH (red) and RH (blue) and covered with water (black), which is the same for both nanostructures. (b) Surface plot of chirality on the top surface.

The simulations, which are intended only as proof of principle, are not exact reproductions of the experimentally observed changes. Since the protein layers are not isotropic in nature, and

orientation plus physical coverage of the proteins cannot be replicated in a simulated environment. The anisotropic nature of the protein layers is important because higher order contributions, such as electric dipole – electric quadrupole, can contribute to optical activity. In contrast optical activity of isotropic layers is only derived from electric dipole – magnetic dipole contributions. The simulations do not incorporate the quadrupolar contribution to the chiral behaviour. Yet they prove the hypothesis that the phase retardation of chiral plasmonic resonators will be dependent on the inherent chirality of the surrounding dielectric environment. Affimers have high β-sheet content (~55%) that have a significant quadrupolar and multipolar contribution to the optical activity that cannot be replicated in a simulated environment.[25,37] Consequently, we speculate that the experimentally observed structural dependency of phase asymmetries is due to the higher order moments.

Conclusion

We present a phenomenon, an asymmetry in the retardation phase changes induced by a differential interaction of LH and RH chiral near fields with a chiral dielectric. The phenomenon is a highly incisive probe being sensitive to structural differences in a family of related proteins with similar secondary and tertiary structure. Phase retardations are obtained using a straightforward parametric curve fit of the EIT line shape in the reflectance spectra. These phase retardations provide fingerprints that enable discrimination of proteins which have similar structures but have primary sequences that differ by a single amino acid (G65C and K67C). The concept that chiral dielectric alter retardation phases from chiral plasmonic nanostructures has been validated by numerical EM modelling, which shows asymmetry in phase shifts from an isotropic chiral media. Although EM modelling are required to validate

the observations in this proof-of-principle study, they are not required for the routine application of phase retardation shifts for sensing biological structure.

Previous work has demonstrated that the introduction of a dielectric changes the amplitude and phase of the near field around a plasmonic nanostructure. These effects have been understood within the framework of circuit theory,[38] with the introduction of the dielectric altering the capacitance of the system. Within this framework, the observed phase asymmetry can be understood by assuming two capacitive coupled oscillators, where the capacitance is dependent on the handedness of both the near fields and the dielectric.

The phase sensitivity measurement presented in this study are a more sensitive probe of the geometric structure of protein layers than previous applications of chiral plasmonic fields. This previous work demonstrated the ability to discriminate between proteins with significantly different secondary structure. The phenomenon is a valuable addition to the bioanalytical tool box since it provides a rapid and simple fingerprint of interfacial structure which would otherwise not be possible. Although simple protein fragments have been used as an exemplar, the phenomenon could readily be applied to more complex biological interfaces. This ability to sense protein layer structure generates useful modalities for sensing, providing a tool for probing tertiary structure in a high-throughput fashion. This approach is particularly promising for monitoring protein homogeneity, as well as providing added dimensionality for sensor arrays.

Methods

Fabrication of templated plasmonic substrates

The templated substrates were prepared by injection moulding as described previously by Karimullah *et al.* and Gadegaard *et al*.[19,23] In brief, clean silicon substrates were coated with 80 nm of PMMA (Elvacite 2041, Lucite International) and exposed in a Vistec VB6 UHR EWF lithography tool operating at 100 kV. After exposure the substrates were developed and a 300 μm thick nickel shim was formed through electroplating. The shim was mounted in a custom made tool capable of manufacturing ASA standard polymer slides. An Engel Victory Tech 28 tons injection moulding machine was used in fully automatic production mode in the manufacture of the polymer slides using polycarbonate (Makrolon DP2015) as feedstock. Polycarbonate is known to have the best ability to replicate the nanofeatures and is commonly used in the industry for optical storage media[39]. The injection moulded substrates have the chiral nanostructures imparted in the plastic surface and are subsequently covered by a continuous 100 nm Au film to complete the TPS process.

Measurement of optical spectra

We have used a custom built polarimeter that measures the reflected light from our samples. It uses a tungsten halogen light source (Thorlabs), calcite polarisers (Thorlabs) and a 10 x objective (Olympus). The samples are positioned with the help of a camera (Thorlabs, DCC1645C) and the spectrum is measured using a compact spectrometer (Ocean optics USB4000). Using Stokes methods, we can measure the intensity of light at four angles of the analyser and calculate the optical properties of our chiral plasmonic arrays. Reflectivity measurements used plain Au as a background reference and the data was fitted using a script

written in Matlab (Mathworks). The errors were determined from the deviation of 8 measurements.

Affimer preparation and experiments

All Affimer stock solutions were obtained from Avacta Life Sciences and diluted to a concentration of 1 mg/ml in 10mM HBS (HEPES buffered saline). Reference measurements were taken from both left and right handed nanostructures in 10 mM HBS only. After reference measurements were taken, the diluted Affimer solution was added to the clean gold slides and left to incubate at room temperature for 2 hours. After incubation, the gold slide was rinsed again with 10 mM HBS to remove any unbound Affimer and measurements were recorded.

Electromagnetic Simulation

EM simulations were performed using a commercial finite-element package (COMSOL v4.4, Wave optics module). Permittivity values for gold were taken from Johnson *et al*.[40] Periodic boundary conditions were used to emulate the array of nanostructures. Perfectly matched layer conditions were used above and below the input and output ports. Linear polarised EM wave was applied at normal incidence onto the structure.

Corresponding Authors: Affar.Karimullah@glasgow.ac.uk, Malcolm.Kadodwala@glasgow.ac.uk

Acknowledgements

The authors acknowledge financial support from the Engineering and Physical Sciences Research Council (EP/K034936/1 & EP/P00086X/1), JSPS Core to Core (EP/M024423/1), and technical support from the James Watt Nanofabrication Centre (JWNC). They would also like to thank Avacta Life Sciences for contributing the Affimer proteins. RT thanks the EPSRC for the award of scholarship, and VR acknowledges support from the National Institutes of Health (GM077173).

Supporting Information Available: Templated Plasmonic Substrates: Fabrication and Properties, EM Simulation, Mathematical Model for EIT, Salt Solution Fitting, Affimers, Protein Fitting Results and ORD measurements, Chiral Simulation Fitting Results.

This material is available free of charge *via* the Internet at http://pubs.acs.org.

References

(1) Dufrêne, Y. F. Using Nanotechniques to Explore Microbial Surfaces. *Nat. Rev. Microbiol.* **2004**, *2*, 451–460.

(2) Okawa, S.; Watanabe, K. Chemical Mechanical Polishing of Titanium with Colloidal Silica Containing Hydrogen Peroxide--Mirror Polishing and Surface Properties. *Dent. Mater. J.* **2009**, *28*, 68–74.

(3) Tang, Y.; Cohen, A. E. Enhanced Enantioselectivity in Excitation of Chiral Molecules

by Superchiral Light. *Science* **2011**, *332*, 333–336.

(4) Tang, Y.; Cohen, A. E. Optical Chirality and Its Interaction with Matter. *Phys. Rev. Lett.* **2010**, *104*, 163901.

(5) Hendry, E.; Carpy, T.; Johnston, J.; Popland, M.; Mikhaylovskiy, R. V; Lapthorn, A. J.; Kelly, S. M.; Barron, L. D.; Gadegaard, N.; Kadodwala, M. Ultrasensitive Detection and Characterization of Biomolecules Using Superchiral Fields. *Nat. Nanotechnol.* **2010**, *5*, 783–787.

(6) Hendry, E.; Mikhaylovskiy, R. V; Barron, L. D.; Kadodwala, M.; Davis, T. J. Chiral Electromagnetic Fields Generated by Arrays of Nanoslits. *Nano Lett.* **2012**, *12*, 3640–3644.

(7) Schäferling, M.; Yin, X.; Engheta, N.; Giessen, H. Helical Plasmonic Nanostructures as Prototypical Chiral Near-Field Sources. *ACS Photonics* **2014**, *1*, 530–537.

(8) Khoo, E. H.; Leong, E. S. P.; Wu, S. J.; Phua, W. K.; Hor, Y. L.; Liu, Y. J. Effects of Asymmetric Nanostructures on the Extinction Difference Properties of Actin Biomolecules and Filaments. *Sci. Rep.* **2016**, *6*, 19658.

(9) Zhao, Y.; Askarpour, A. N.; Sun, L.; Shi, J.; Li, X.; Alù, A. Chirality Detection of Enantiomers Using Twisted Optical Metamaterials. *Nat. Commun.* **2017**, *8*, 14180.

(10) Tullius, R.; Karimullah, A. S.; Rodier, M.; Fitzpatrick, B.; Gadegaard, N.; Barron, L. D.; Rotello, V. M.; Cooke, G.; Lapthorn, A.; Kadodwala, M. "Superchiral" Spectroscopy: Detection of Protein Higher Order Hierarchical Structure with Chiral Plasmonic Nanostructures. *J. Am. Chem. Soc.* **2015**, *137*, 8380–8383.

(11) Davis, T. J.; Vernon, K. C.; Gómez, D. E. Effect of Retardation on Localized Surface Plasmon Resonances in a Metallic Nanorod. *Opt. Express* **2009**, *17*, 23655–23663.

(12) Davis, T. J. *Colloquium*: An Algebraic Model of Localized Surface Plasmons and Their Interactions. *Rev. Mod. Phys.* **2017**, *89*, 11003.

(13) Maier, S. A. *Plasmonics: Fundamentals and Applications*; Springer US: New York, 2007.

(14) Imamoglu, A.; Boller, K. J.; Harris, S. E. Electromagnetically Induced Transparency. *Phys. Today* **1997**, *50*, 36–42.

(15) Fleischhauer, M.; Imamoglu, A.; Marangos, J. Electromagnetically Induced Transparency: Optics in Coherent Media. *Rev. Mod. Phys.* **2005**, *77*, 633–673.

(16) Zhang, S.; Genov, D. A.; Wang, Y.; Liu, M.; Zhang, X. Plasmon-Induced Transparency in Metamaterials. *Phys. Rev. Lett.* **2008**, *101*, 47401.

(17) Liu, N.; Langguth, L.; Weiss, T.; Kästel, J.; Fleischhauer, M.; Pfau, T.; Giessen, H. Plasmonic Analogue of Electromagnetically Induced Transparency at the Drude Damping Limit. *Nat. Mater.* **2009**, *8*, 758–762.

(18) Taubert, R.; Hentschel, M.; Kästel, J.; Giessen, H. Classical Analog of Electromagnetically Induced Absorption in Plasmonics. *Nano Lett.* **2012**, *12*, 1367–1371.

(19) Karimullah, A. S.; Jack, C.; Tullius, R.; Rotello, V. M.; Cooke, G.; Gadegaard, N.; Barron, L. D.; Kadodwala, M. Disposable Plasmonics: Plastic Templated Plasmonic Metamaterials with Tunable Chirality. *Adv. Mater.* **2015**, *27*, 5610–5616.

(20) Jack, C.; Karimullah, A. S.; Leyman, R.; Tullius, R.; Rotello, V. M.; Cooke, G.; Gadegaard, N.; Barron, L. D.; Kadodwala, M. Biomacromolecular Stereostructure Mediates Mode Hybridization in Chiral Plasmonic Nanostructures. *Nano Lett.* **2016**, *16*, 5806–5814.

(21) Liu, N.; Weiss, T.; Mesch, M.; Langguth, L.; Eigenthaler, U.; Hirscher, M.; Sönnichsen, C.; Giessen, H. Planar Metamaterial Analogue of Electromagnetically Induced Transparency for Plasmonic Sensing. *Nano Lett.* **2010**, *10*, 1103–1107.

(22) Hentschel, M.; Weiss, T.; Bagheri, S.; Giessen, H. Babinet to the Half: Coupling of Solid and Inverse Plasmonic Structures. *Nano Lett.* **2013**, *13*, 4428–4433.

(23) Gadegaard, N.; Mosler, S.; Larsen, N. B. Biomimetic Polymer Nanostructures by Injection Molding. *Macromol. Mater. Eng.* **2003**, *288*, 76–83.

(24) Tassin, P.; Zhang, L.; Zhao, R.; Jain, A.; Koschny, T.; Soukoulis, C. M. Electromagnetically Induced Transparency and Absorption in Metamaterials: The Radiating Two-Oscillator Model and Its Experimental Confirmation. *Phys. Rev. Lett.* **2012**, *109*, 1–5.

(25) Tiede, C.; Tang, A. A. S.; Deacon, S. E.; Mandal, U.; Nettleship, J. E.; Owen, R. L.; George, S. E.; Harrison, D. J.; Owens, R. J.; Tomlinson, D. C.; McPherson, M. J. Adhiron: A Stable and Versatile Peptide Display Scaffold for Molecular Recognition Applications. *Protein Eng. Des. Sel.* **2014**, *27*, 145–155.

(26) Jack, C.; Karimullah, A. S.; Tullius, R.; Khorashad, L. K.; Rodier, M.; Fitzpatrick, B.; Barron, L. D.; Gadegaard, N.; Lapthorn, A. J.; Rotello, V. M.; Cooke, G.; Govorov, A. O.; Kadodwala, M. Spatial Control of Chemical Processes on Nanostructures through Nano-Localized Water Heating. *Nat. Commun.* **2016**, *7*, 10946.

(27) Woodman, R.; Yeh, J. T. H.; Laurenson, S.; Ko Ferrigno, P. Design and Validation of a Neutral Protein Scaffold for the Presentation of Peptide Aptamers. *J. Mol. Biol.* **2005**, *352*, 1118–1133.

(28) Hoffmann, T.; Stadler, L. K. J.; Busby, M.; Song, Q.; Buxton, A. T.; Wagner, S. D.;

Davis, J. J.; Ko Ferrigno, P. Structure-Function Studies of an Engineered Scaffold Protein Derived from Stefin A. I: Development of the SQM Variant. *Protein Eng. Des. Sel.* **2010**, *23*, 403–413.

(29) Estrela, P.; Paul, D.; Migliorato, P.; Ferrigno, P. K.; Wang, L.; Huq, E. Potentiometric Detection of Protein Interactions with Peptide Aptamers. *Proc. IEEE Sensors* **2008**, 646–649.

(30) Ferrigno, P. K. Non-Antibody Protein-Based Biosensors. *Essays Biochem.* **2016**, *60*, 19–25.

(31) Johnson, A.; Song, Q.; Ko Ferrigno, P.; Bueno, P. R.; Davis, J. J. Sensitive Affimer and Antibody Based Impedimetric Label-Free Assays for C-Reactive Protein. *Anal. Chem.* **2012**, *84*, 6553–6560.

(32) Cho, K. Dispersion Relation in Chiral Media: Credibility of Drude-Born-Fedorov Equations. **2015**, *1*, 1–7.

(33) Govorov, A. O.; Fan, Z.; Hernandez, P.; Slocik, J. M.; Naik, R. R. Theory of Circular Dichroism of Nanomaterials Comprising Chiral Molecules and Nanocrystals: Plasmon Enhancement, Dipole Interactions, and Dielectric Effects. *Nano Lett.* **2010**, *10*, 1374–1382.

(34) Govorov, A. O.; Fan, Z. Theory of Chiral Plasmonic Nanostructures Comprising Metal Nanocrystals and Chiral Molecular Media. *Chemphyschem* **2012**, *13*, 2551–2560.

(35) Abdulrahman, N. A.; Fan, Z.; Tonooka, T.; Kelly, S. M.; Gadegaard, N.; Hendry, E.; Govorov, A. O.; Kadodwala, M. Induced Chirality through Electromagnetic Coupling between Chiral Molecular Layers and Plasmonic Nanostructures. *Nano Lett.* **2012**, *12*, 977–983.

(36) Davis, T. J.; Hendry, E. Superchiral Electromagnetic Fields Created by Surface Plasmons in Nonchiral Metallic Nanostructures. *Phys. Rev. B* **2013**, *87*, 85405.

(37) Barron, L. D. *Molecular Light Scattering and Optical Activity*; Cambridge University Press: Cambridge, 2009.

(38) Schnell, M.; García-Etxarri, A.; Huber, A. J.; Crozier, K.; Aizpurua, J.; Hillenbrand, R. Controlling the near-Field Oscillations of Loaded Plasmonic Nanoantennas. *Nat. Photonics* **2009**, *3*, 287–291.

(39) Monkkonen, K.; Pakkanen, T. T.; Hietala, J.; Paakkonen, E. J.; Paakkonen, P.; Jaaskelainen, T.; Kaikuranta, T. Replication of Sub-Micron Features Using Amorphous Thermoplastics. *Polym. Eng. Sci.* **2002**, *42*, 1600–1608.

(40) Johnson, P.; Christy, R. Optical Constants of the Noble Metals. *Phys. Rev. B* **1972**, *6*, 4370–4379.